


Broadband, Flat-Top, Silicon Photonic Contra-Directional Couplers Assisted by Asymmetric Multimode Photonic Crystals

Ronglei Sun, Qi Wang, Wenkang Wang, and Rui Cheng 

Abstract—Grating-assisted contra-directional couplers (CDCs) as 4-port wavelength-selective devices hold great potential as add-drop filters, multiplexers, routers, etc, for various integrated-optics applications. However, these devices have inherent low coupling strengths due to the coupled modes confined in different separate waveguides, preventing from realizing broad operation bands. Here, we propose silicon photonic CDCs assisted by novel asymmetric photonic crystals (APhCs) on multimode waveguides with elliptical nanoholes. Such APhC-assisted CDCs, compared with the conventional grating-assisted ones, can achieve significantly larger coupling strengths, thus offering much wider operation bands. We investigate the impact of changes in various structural parameters on the spectral response of an APhC-assisted CDC, and then discuss the design and optimization strategy of the device. The possibility of using other nanohole shapes of the APhC is also explored. In the experiments, a series of broadband and flat-top filters based on APhC-assisted CDCs on silicon-on-insulator (SOI) were fabricated and measured, and the influence of variations in the filter parameters on the response was validated. Notably, a 3 dB bandwidth of ~ 48.8 nm was demonstrated on an APhC-assisted CDC with a coupling length of 22.3 μm , which is the largest bandwidth ever reported for unchirped, SOI-based CDC filters, to the best of our knowledge.

Index Terms—Asymmetric photonic crystals, broadband filtering, contra-directional couplers.

I. INTRODUCTION

INTEGRATED waveguide Bragg gratings based on silicon-on-insulator (SOI) platforms have advantages of low insertion losses, high extinction ratios, flexible spectral responses, and CMOS compatibility. They have been used in various integrated-optics applications including optical telecommunications [1], [2], sensing [3], laser engineering [4], and microwave

photonics [5], and can act as versatile filters [6], multiplexers [7], mode converters [8], dispersion compensators [9], photonic signal processors [10], etc. Waveguide Bragg gratings typically work in the reflection mode. Thus, for traditional single waveguide-based Bragg gratings, which are 2-port devices, an optical circulator or 3 dB splitter is generally required to be placed before the device to extract the reflected signal separately [6]. Such a configuration, however, can introduce additional insertion loss and complexity to the system. To address this issue, grating-assisted contra-directional couplers (CDCs), which have 4 ports, have been emerged in recent years [11]. For these filters, the contra-directional coupling happens between modes confined in different separate waveguides, and thus the reflection will ultimately exit through the output of another waveguide, eliminating the need to use extra devices to extract the reflected signal. Also, such 4-port filters provide an additional useful signal add-drop functionality, which can be used to realize add-drop filters, multiplexers, routers, etc. However, due to the high index contrast of an SOI waveguide, the two coupled modes for a grating-assisted CDC are generally strongly confined in the two separate waveguides. This means that the overlap between the coupled modes within the structure perturbation region is small. As a result, the coupling strength of a grating-assisted CDC is typically low, which prevents from achieving broad operation bands using such devices [12]. Specifically, as shown in Fig. 3(a) in [13], even with large corrugation widths of 50 nm and 30 nm of the wider and narrower waveguide gratings, respectively, and a small waveguide gap of only 50 nm, the 3 dB bandwidth of the resulting grating-assisted CDC filter is still only about 3 nm. This issue has restricted the use of these devices in wide-band applications.

Considerable efforts have been made to increase the coupling strength and thus the bandwidth of a grating-assisted CDC filter. A straightforward concept is to decrease the field confinements of the two coupled modes, which can be realized by using sub-wavelength grating (SWG) waveguides. Naghdi et al. presented a CDC where one of the waveguides was replaced by a SWG waveguide [14]. Besides the less confinement of the modes in a SWG waveguide, the SWG itself also provided the required grating mechanism, where the strong on/off grating led to a relatively high coupling strength. Through that method, a bandwidth of about 21 nm with a filter length of 50 μm was realized. Later on, Charron et al. in 2018 proposed a broadband

Manuscript received 2 September 2023; revised 2 November 2023; accepted 24 November 2023. Date of publication 29 November 2023; date of current version 11 December 2023. This work was supported in part by the National key research and development program of China under Grant 2021YFB2801500, in part by the National Natural Science Foundation of China under Grant 62105089, and in part by the Project of Key Laboratory of Radar Imaging and Microwave Photonics (Nanjing University of Aeronautics and Astronautics), Ministry of Education under Grant NJ20210003. (Corresponding author: Rui Cheng.)

The authors are with the School of Instrument Science and Optoelectronics Engineering, Hefei University of Technology, Hefei, Anhui 230009, China (e-mail: rlsun@mail.hfut.edu.cn; 1048309339@qq.com; wangwenkang@mail.hfut.edu.cn; rcheng@hfut.edu.cn).

Digital Object Identifier 10.1109/JPHOT.2023.3337395

CDC filter where a novel sidewall-corrugated SWG waveguide was utilized to further increase the coupling strength [15]. In that work, a record large bandwidth of 4.07 THz (33.4 nm) was achieved experimentally. Yun et al. proposed a novel CDC filter consisting of two sidewall-corrugated SWG waveguides to increase the coupling strength, and also employed the corrugation width apodization method to suppress the side-lobe of the spectrum [12]. A filter with a 3 dB bandwidth of 32.6 nm and a side-lobe suppression ratio of 19 dB was obtained through that scheme. Nevertheless, although the use of SWG waveguides can effectively increase the bandwidth of a grating-assisted CDC filter, the SWG structures have small feature spacing and size that may be challenging to be precisely fabricated by standard photolithography. Another method to address the bandwidth limitation of a grating-assisted CDC is to introduce a period chirp along the grating, but this will also largely increase the device length. Hammood et al. reported a CDC filter based on a chirped grating which can achieve a large bandwidth up to 88.1 nm [16], but the corresponding device length is as long as 3200 μm . Therefore, there still lacks an effective method to significantly increase the coupling strength of a CDC filter while at the same time allowing the device to be easily fabricated and compact.

In this article, we describe a new kind of silicon photonic, wavelength-selective, contra-directional coupler which is assisted by a novel asymmetric photonic crystal (APhC) that is developed on a multimode waveguide and has elliptical nanoholes. Such APhC-assisted CDCs possess significantly larger coupling strengths and thus wider bandwidths compared with previous types of wavelength-selective CDC, including those based on sidewall-modulated gratings [11], [13] and SWG waveguides [12], [14], [15]. Furthermore, the proposed CDCs have compact sizes, and contain relatively large feature sizes and spacing and thus could be easily fabricated. We investigate the impact of variations in important structure parameters on the spectral response of an APhC-assisted CDC, and then discuss the design and optimization strategy of the device. In the experiments, a number of broadband and flat-top APhC-assisted CDC filters based on SOI platforms were fabricated and tested, and the influence of changes in the parameters on the filter response was validated. APhC-assisted CDCs with other shapes of the nanoholes, including rectangular, sinusoidal, diamond, and circular, were also designed and experimentally characterized. Notably, a 3 dB bandwidth of ~ 48.8 nm is demonstrated based on a ~ 22 μm -long APhC-assisted CDC, which is the largest bandwidth among the reported unchirped SOI-based CDC filters, to the best of our knowledge. The proposed APhC-assisted CDCs can be potentially used to filter single (such as the C-band) or multiple wavelength bands for wavelength-division multiplexing (WDM) band splitting, and can also operate as wavelength-band multiplexers/demultiplexers in ultra-broadband silicon photonic circuits.

II. PRINCIPLE AND DESIGN

A. Basic Principle

The devices described in this work are developed on 220-nm-high strip SOI waveguides with a silicon dioxide

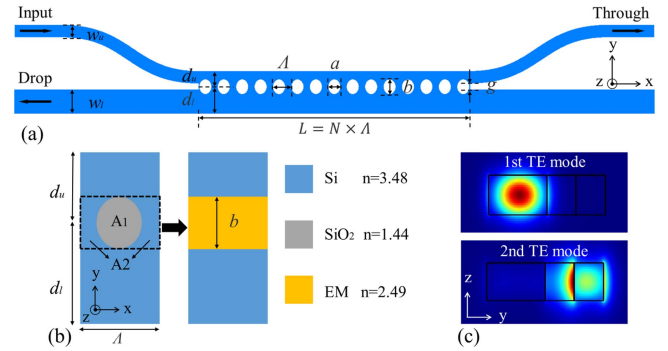


Fig. 1. (a) Top view of an APhC-assisted CDC. (b) Schematic illustration of the equivalent three-medium system. (c) Cross-sectional optical field distributions of the (upper) 1st and (lower) 2nd TE system modes.

cladding layer deposited on the waveguides. A schematic top view of our proposed APhC-assisted CDC is shown in Fig. 1(a). The APhC-assisted CDC consists of an asymmetric photonic crystal built on a multimode waveguide and input/output access waveguides with S-bend structures. The APhC is essentially a multimode waveguide with off-center periodic elliptical SiO_2 nanoholes. The important parameters of the devices are the widths of the upper and lower access waveguides (w_u and w_l , respectively), the vertical distance between the center of the nanoholes and the upper or lower edge of the multimode waveguide (the smaller or larger one of the two distances will be denoted by d_u or d_l , respectively), the period of the APhC (Λ), the widths and heights of the elliptical holes (a and b , respectively), the total number of the periods of the APhC (N), and the minimum gap between the access waveguides (g).

The photonic crystal region, according to the effective medium theory [17], can be considered as a material whose effective index is intermediate between those of Si and SiO_2 . In this way, the multimode waveguide can be regarded as a three-medium system [Fig. 1(b)], The effective index of the middle medium can be estimated by [17]:

$$n_{EM}^2 \cdot (A_1 + A_2) = n_{\text{SiO}_2}^2 \cdot A_1 + n_{\text{Si}}^2 \cdot A_2 \quad (1)$$

where n_{Si} and n_{SiO_2} are the refractive indices of Si and SiO_2 , respectively; A_1 is the area of the elliptical hole, which can be expressed by $A_1 = \pi ab/4$; and A_2 is the area of the region enclosed by the dashed box excluding the SiO_2 hole in Fig. 1(b), which can be calculated via $A_2 = b \cdot \Lambda - A_1$. Such a three-medium system have the 1st and 2nd transverse electric (TE) system modes mainly confined in the wider and narrower Si regions of the multimode waveguides, as shown in Fig. 1(c).

In addition to acting as the middle medium of the waveguide system, the APhC itself also provides a periodic structural perturbation between the two system modes, and thus allows contra-directional coupling between them. In order to ensure that this coupling happens near a designed wavelength, λ_0 , the following phase matching condition should be satisfied [18]:

$$(n_0 + n_1)\Lambda = \lambda_0 \quad (2)$$

where n_0 and n_1 are the effective refractive indices of the 1st and 2nd TE modes of the three-medium system, respectively.

When the upper narrower access waveguide is used as the input [which is the case illustrated in Fig. 1(a)], the input mode will be adiabatically evolved into the 2nd system mode of the multimode waveguide, and then will be coupled to the backward 1st system mode due to the periodic structural perturbation induced by the APhC. This backward signal will be adiabatically evolved into the fundamental mode of the lower wider access waveguide, and finally exit through the drop port of the CDC. The device can also work based on a similar mechanism when the lower wider access waveguide is used as the input.

The APhC, due to its large periodic elliptical SiO₂ nanoholes, offers an extremely large perturbation between the two system modes, which will bring about high coupling strength between these modes. Furthermore, as the photonic crystal region can be considered as a medium whose effective index is intermediate between those of Si and SiO₂, this can reduce the effective index contrast of the waveguide, and thus decrease the confinement of the two system modes. This is illustrated in Fig. 1(c), where it can be clearly seen that the 2nd TE system mode is not well-confined with a considerable portion of the mode energy located in the perturbation region. Such a smaller mode confinement can increase the overlap between the two coupled mode, thereby significantly increasing the coupling strength. Owing to these reasons, the APhC-assisted CDC can easily achieve a significantly larger coupling strength over a conventional grating-assisted CDC. For a one-dimensional PhC like the APhC used here, its bandwidth is strongly dependent on the coupling strength (κ) with the following relationship [19]:

$$\Delta\lambda = \frac{\lambda_B^2}{\pi n_g} \sqrt{\kappa^2 + \left(\frac{\pi}{L}\right)^2} \quad (3)$$

where $\Delta\lambda$ is the reflection bandwidth between the first nulls around the center wavelength, λ_B is the center wavelength (or the Bragg wavelength) of the PhC, L is the coupling length, and n_g is the group index. Therefore, the proposed APhC-assisted CDCs due to their large coupling strengths will offer broad, flat-top filtering responses. It is important to note that the degree of asymmetry of the APhC (or the difference between d_u and d_l) needs to be large enough to 1) minimize directional mode coupling, and 2) ensure that the reflection bands due to the contra-directional coupling between the same order modes are not overlapped with the operation band.

To proof the functionality of our device, an APhC-assisted CDC based broadband and flat-top filter centered around the wavelength of 1550 nm is designed and its spectral response is characterized using the three-dimensional finite difference time-domain (3D-FDTD) method. The parameters of the APhC-assisted CDC have been decided based on the design and optimization methodology detailed in Section II-C of this paper. For the designed filter, d_u and d_l are 0.45 μm and 0.75 μm , respectively; a and b are 0.24 μm and 0.3 μm , respectively; Λ is 320 nm; and N is 70, translating to an APhC length of 22.4 μm . The equivalent refractive index of the middle medium of the waveguide system estimated from (1) is about 2.49. The effective refractive indices of the 1st and 2nd TE system modes are then calculated to be $n_0 = 2.18$ and $n_1 = 2.61$, respectively.

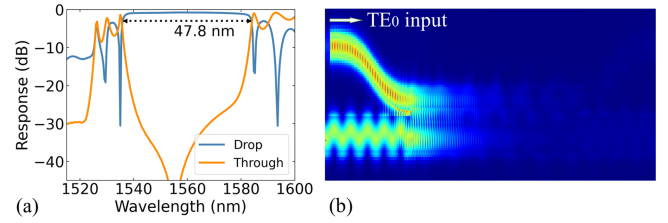


Fig. 2. (a) Simulated drop and through responses of an APhC-assisted CDC. (b) Electric field distribution over the CDC when the light with the TE₀ mode at a wavelength of 1558 nm is injected from the input port.

The simulated cross-sectional electric intensity distributions of the 1st and 2nd TE system modes are shown in Fig. 1(c). It should be noted that w_u , w_l , and g need to be chosen such that the effective indices of the strip waveguide modes and the Bloch modes in the APhC-assisted CDCs are close to each other to minimize the transmission loss and spectral distortion due to the mode mismatch. According to this view, w_u , w_l and g are set to 0.4 μm , 0.7 μm , and 0.1 μm , respectively. Note that the current value of g may not be manufacturable by standard photolithography. Nevertheless, this can potentially be addressed by using a larger width of the multimode waveguide, which can allow a larger g to be used in the design.

The drop and through responses of the designed filter calculated from the 3D-FDTD are shown in Fig. 2(a). The filter has a wide and flat-top drop response with a 3 dB bandwidth of 47.8 nm. The maximum extinction ratio (ER), defined as the ratio of the drop-port power to the through-port power, is about 51 dB at the wavelength of 1555 nm. One may notice from the through response that there is another unintended stop band at the shorter wavelength side of the operation band, which is caused by the coupling between the backward and forward 2nd system modes. The filter needs to be designed so that the reflection bands due to such coupling will not overlap with the intended operation band. Fig. 2(b) shows the electric field distribution of the device when the light with the fundamental TE₀ mode at a wavelength of 1558 nm is injected from the input port of the CDC. It can be seen that the light is directed to the drop port, with no appreciable light traveling to the other ports.

B. Impact of Changes in Various Parameters on the Response of an APhC-Assisted CDC

In this section, we investigate the influence of variations in different parameters on the spectral response of an APhC-assisted CDC. The calculations are performed using the 3D-FDTD method.

1) *Vertical Distances Between the Nanoholes and Both Edges of the Multimode Waveguide (d_l and d_u):* We first study how various vertical distances between the nanoholes and the lower or upper edge of the multimode waveguide can affect the spectral response of the proposed CDC. Note again that here d_l or d_u denotes the larger or smaller one of the two distances, respectively. First the impact due to variations in d_l is studied. We design a series of APhC-assisted CDCs which have the same d_u of 0.45 μm but different d_l of 0.65 μm , 0.7 μm , 0.8 μm , and 0.85 μm .

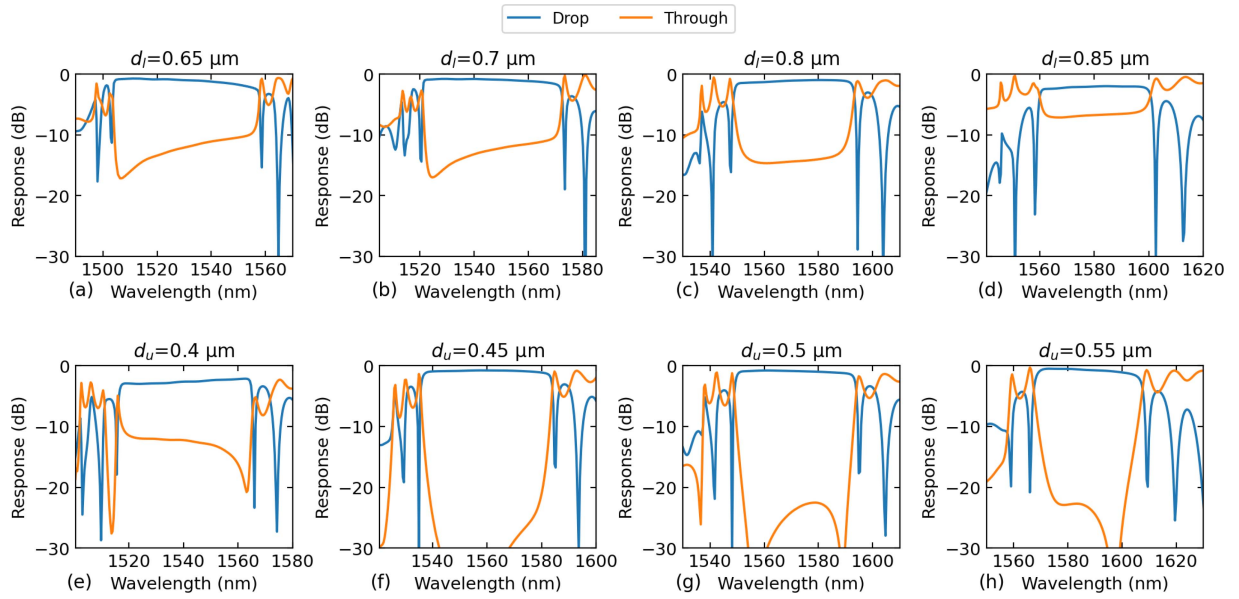


Fig. 3. Simulated responses of APhC-assisted CDCs with (a)–(d) different d_l or (e)–(h) various d_u . For the other parameters, $d_u = 0.45 \mu\text{m}$ [in (a)–(d)], $d_l = 0.75 \mu\text{m}$ [in (e)–(h)], $a = 0.24 \mu\text{m}$, $b = 0.3 \mu\text{m}$, $w_u = 0.4 \mu\text{m}$, $g = 0.1 \mu\text{m}$, $N = 70$, $\Lambda = 0.32 \mu\text{m}$, and w_l is changed with d_l or d_u to ensure that g remains unchanged at $0.1 \mu\text{m}$.

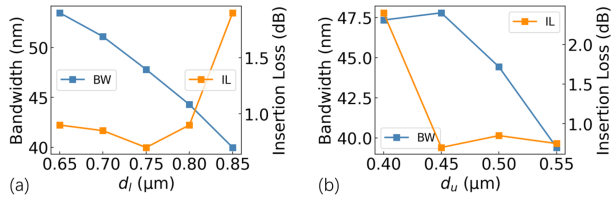


Fig. 4. 3 dB bandwidth and insertion loss of an APhC-assisted CDC as a function of (a) d_l and (b) d_u , extracted from the simulation data shown in Fig. 3.

For the other parameters, $a = 0.24 \mu\text{m}$, $b = 0.3 \mu\text{m}$, $w_u = 0.4 \mu\text{m}$, $g = 0.1 \mu\text{m}$, $N = 70$, and $\Lambda = 320 \text{ nm}$. Note that w_l is changed with d_l to ensure that g remains unchanged at $0.1 \mu\text{m}$. The simulated responses of the filters are shown in Fig. 3(a)–(d), and the extracted 3 dB bandwidth and insertion loss as a function of d_l is plotted in Fig. 4(a). It can be seen that the bandwidth of the filter decreases with increasing d_l . This is because when d_l is larger, the 1st TE system mode will be more confined in the wider Si region of the multimode waveguide, resulting in a decrease of the overlap between the coupled modes. This will reduce the mode coupling strength, and thus decrease the bandwidth. One may also notice that the insertion loss of the reflection for the largest d_l of $0.85 \mu\text{m}$ is noticeably higher than those with smaller d_l , and the ER for this filter is also lower than those of the other cases. This could be due to that, in this case, the multimode waveguide supports more high-order modes, and thus may cause a larger portion of the forward 2nd TE system mode (that is the input light) coupled to higher-order modes.

Then to investigate how different d_u can affect the CDC response, APhC-assisted CDCs that have the same d_l of $0.75 \mu\text{m}$ but different d_u of $0.4 \mu\text{m}$, $0.45 \mu\text{m}$, $0.5 \mu\text{m}$, and $0.55 \mu\text{m}$ are characterized. The simulation results are presented in

Fig. 3(e)–(h), and the extracted 3 dB bandwidth and insertion loss as a function of d_u is plotted in Fig. 4(b). It can be observed that the bandwidth is decreased as d_u is increased. This is because a larger d_u can increase the mode confinement of the 2nd TE system mode, which decreases the overlap between the coupled modes, thereby reducing the mode coupling strength and thus the bandwidth. It can also be noticed that for the CDC with the lowest d_u of $0.4 \mu\text{m}$, the insertion loss of the drop signal is larger and the ER is smaller compared with those of the others. This could be attributed to that when d_u is too small, a considerable portion of the field of the 2nd TE system mode is located in the nanohole region, leading to a significant scattering loss.

2) *Widths (a) and Heights (b) of the Elliptical Nanoholes:* The impact of changes in the widths and heights of the elliptical nanoholes on the spectral response of the CDC is now investigated. We designed and characterized a series of the filters with various a and b . For other parameters of the filters, $w_u = 0.4 \mu\text{m}$, $w_l = 0.7 \mu\text{m}$, $d_u = 0.45 \mu\text{m}$, $d_l = 0.75 \mu\text{m}$, $g = 0.1 \mu\text{m}$, $N = 70$, and $\Lambda = 320 \text{ nm}$. We first study the impact due to changes in a . The simulated responses of the CDCs when a is changed from $0.2 \mu\text{m}$ to $0.28 \mu\text{m}$ with $b = 0.3 \mu\text{m}$ are plotted in Fig. 5(a)–(d). The corresponding bandwidth and insertion loss as a function of a is presented in Fig. 6(a). As can be seen, the bandwidth is significantly decreased as a is increased. This could be because a can affect the effective duty cycle of the APhC. When a is increased from 0.2 to $0.28 \mu\text{m}$, the effective duty cycle of the PhC is closer to 1 given the period of 320 nm of the APhC used here, which in turn decreases the coupling strength and thus the bandwidth [20].

We then investigate the influence of different heights of the elliptical nanoholes, b , on the spectral response of the CDC. Fig. 5(e)–(h) present the spectral evolution of the CDC when

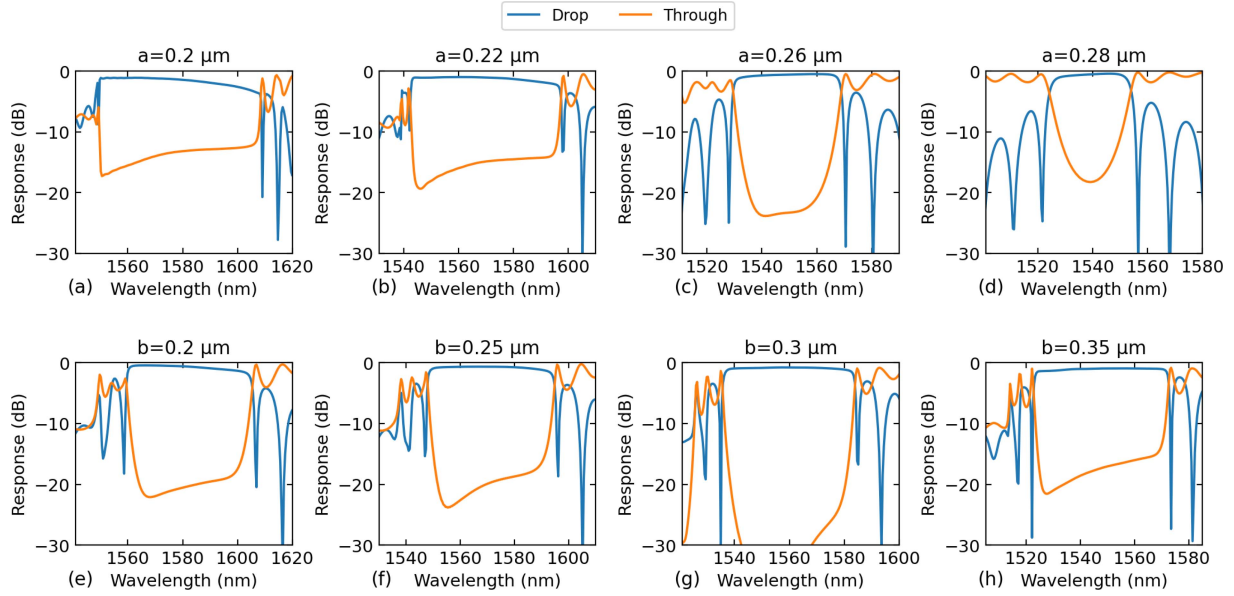


Fig. 5. Simulated responses of APhC-assisted CDCs with (a)–(d) different widths (a) or (e)–(h) various heights (b) of the elliptical nanoholes. For the other parameters, $b = 0.3 \mu\text{m}$ [in (a)–(d)], $a = 0.24 \mu\text{m}$ [in (e)–(h)], $w_u = 0.4 \mu\text{m}$, $w_l = 0.7 \mu\text{m}$, $d_u = 0.45 \mu\text{m}$, $d_l = 0.75 \mu\text{m}$, $g = 0.1 \mu\text{m}$, $N = 70$, and $\Lambda = 0.32 \mu\text{m}$.

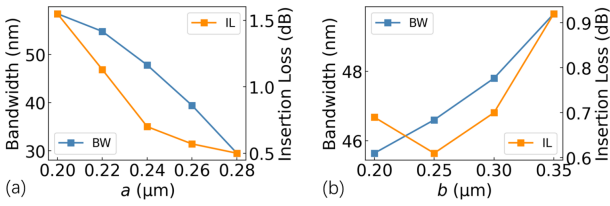


Fig. 6. 3 dB bandwidth and insertion loss of an APhC-assisted CDC as a function of (a) width (a) and (b) height (b) of the elliptical nanoholes, extracted from the simulation data shown in Fig. 5.

varying b of the elliptical nanoholes, from $0.2 \mu\text{m}$ to $0.35 \mu\text{m}$, with a fixed at $0.24 \mu\text{m}$, and Fig. 6(b) shows the extracted bandwidth and insertion loss as a function of b . Only a small increase of the bandwidth is observed as b becomes larger. However, the ERs for various b are significantly different from each other, and the ER for $b = 0.3 \mu\text{m}$ is noticeably larger than those in the other cases. These results indicate that b should be carefully chosen to optimize the ER of the filter.

3) *Minimum Gap Between the Access Waveguides (g):* The impact of various minimum gaps between the access waveguides, g , on the filter response is explored. For an APhC-assisted CDC, g is determined by w_u , w_l , d_u , and d_l by the following equation:

$$g = (d_u + d_l) - (w_u + w_l) \quad (4)$$

Here, to investigate the influence of different g on the filter response, we design and characterize the CDCs with various w_u and w_l but the same d_u and d_l of $0.45 \mu\text{m}$ and $0.75 \mu\text{m}$, respectively. w_u and w_l of these filters are $0.415 \mu\text{m}$ and $0.725 \mu\text{m}$, $0.4 \mu\text{m}$ and $0.7 \mu\text{m}$, $0.38 \mu\text{m}$ and $0.67 \mu\text{m}$, and $0.37 \mu\text{m}$ and $0.63 \mu\text{m}$, which corresponds to various g of $0.06 \mu\text{m}$, $0.1 \mu\text{m}$,

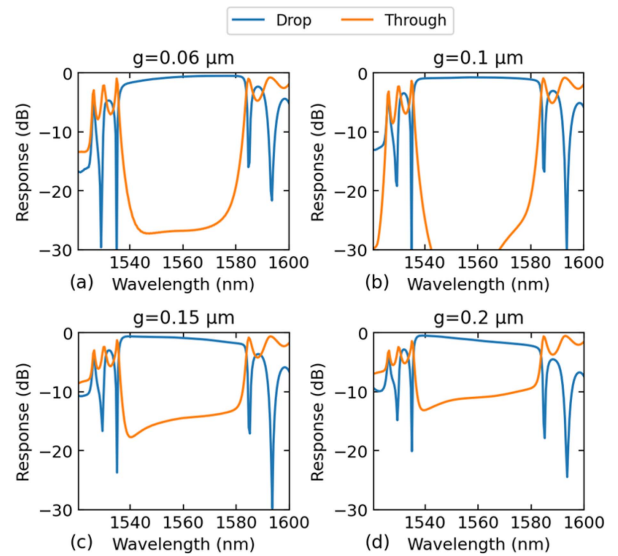


Fig. 7. Simulated responses of APhC-assisted CDCs with different minimum gaps (g) between the access waveguides; g is changed by using various w_u and w_l . For the other parameters, $a = 0.24 \mu\text{m}$, $b = 0.3 \mu\text{m}$, $d_u = 0.45 \mu\text{m}$, $d_l = 0.75 \mu\text{m}$, $N = 70$, and $\Lambda = 0.32 \mu\text{m}$.

$0.15 \mu\text{m}$, and $0.2 \mu\text{m}$, respectively. The 3D-FDTD simulation results of the filters are plotted in Fig. 7. It can be seen that g does not have a significant impact on the bandwidth of the filter. However, it can largely affect the ER. The maximum ERs of the filters with g of $0.06 \mu\text{m}$, $0.1 \mu\text{m}$, $0.15 \mu\text{m}$, and $0.2 \mu\text{m}$, are 27 dB, 45 dB, 14 dB, and 11 dB, respectively. One may also notice that different values of g can also affect the tilt angle of the response. For $g = 0.1 \mu\text{m}$, the top of the drop response is flat, while when $g < 0.1 \mu\text{m}$ and when $g > 0.1 \mu\text{m}$, the tops

are tilted towards shorter and longer wavelengths, respectively. These results indicate that g can be used to optimize the ER and flatness of the response.

C. General Design and Optimization Methodology

By analyzing the simulation results above, we can discuss the design and optimization strategy of the proposed APhC-assisted CDCs. As shown above, the width of the nanoholes (a) and the vertical distances between the nanoholes and both edges of the multimode waveguide (d_u or d_l), compared with other parameters, have relatively larger impacts on the coupling strength and thus the bandwidth of the filter. The minimum gap between the access waveguides (g) and the heights of the nanoholes (b) would not considerably affect the filter bandwidth, but can influence the ER and the flatness of the drop response. Therefore, to design a specific filter based on an APhC-assisted CDC, we can first adjust a , d_u and d_l to roughly tune the bandwidth until it is close to the target value. Then, the other parameters, including g and b , can be finely tuned to improve the flatness of the response and the ER. Note that a too large d_l could lead to a large insertion loss and small ER, which could be due to more energy of the input mode coupled to higher order modes. An overly small d_u could also increase the loss and reduce the ER, which may be attributed to the increased scattering loss. Also, it is important to point out that the degree of the asymmetry of the APhC, i.e., the difference between d_u and d_l , is needed to be large enough to minimize directional mode coupling and also to guarantee that the undesired reflection bands due to the contra-directional coupling between the same order modes are not overlapped with the operation band which comes from the cross mode coupling.

D. APhC-Assisted CDCs With Other Shapes of the Nanoholes

The design and optimization method discussed above are based on APhC-assisted CDCs with elliptical nanoholes. Now, we show that the method can also be used to design the devices with other shapes of the nanoholes. The shapes studied here include rectangular, circular, diamond and sinusoidal, which are schematically illustrated in Fig. 8. We use each of these nanohole shapes to design an APhC-assisted CDC with a broad bandwidth ranging from 35 nm to 45 nm, while having a flat-top drop response and a high ER at the same time. These filters are designed and optimized based on the strategy discussed in the last section. The calculated responses for the various nanohole shapes of the APhC are shown in Fig. 8. It can be found that a broadband and flat-top filter can be achieved for each shape of the nanoholes, which demonstrates the feasibility of the design and optimization method described above. However, it can also be noticed that the ERs obtained for the filters with the various nanohole shapes are different, and are all smaller than that achieved in the elliptical shape case shown in Fig. 2(a) which has a maximum ER of ~ 51 dB. The results suggest that the elliptical shape may bring about better spectral performances and thus be a preferred option for our APhC-assisted CDCs.

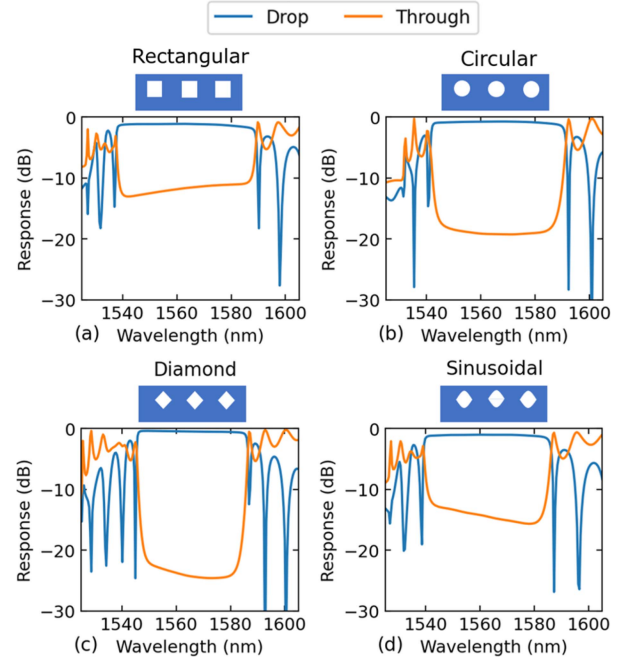


Fig. 8. Simulated responses of APhC-assisted CDCs with different shapes of the nanoholes.

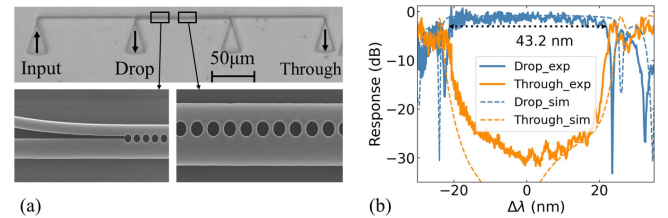


Fig. 9. (a) (Top) optical microscope image of a fabricated integrated-optics circuit for testing the CDC and (bottom) SEM images of various regions of a fabricated APhC-assisted CDC. (b) Measured responses of the APhC-assisted CDC designed in Fig. 2(a).

III. EXPERIMENTAL RESULTS

The designed devices were fabricated based on electron-beam lithography in Applied Nanotools, Inc, using a single etch process on an SOI wafer with 220 nm thick silicon on a 3 μm thick buried oxide layer. A 2 μm thick silicon dioxide cladding layer was deposited on the etched sample, which was performed using a plasma-enhanced chemical vapour deposition (PECVD) process. An optical microscope image of an integrated-optics circuit used for testing an APhC-assisted CDC filter is shown at the top of Fig. 9(a). Four vertical grating couplers (GCs) from the foundry Process Design Kit (PDK), spaced on 127 μm centers, were used to couple light into and out of the chip from a 8-degree polished single-mode optical fiber array with a 127- μm fiber-to-fiber pitch. The scanning electron microscopy (SEM) images of various regions of a fabricated APhC-assisted CDC are shown at the bottom of Fig. 9(a). A tunable laser source (Keysight 81960 A) and a multi-channel optical power sensor (Keysight N7745 A) were used to measure the spectral responses of the CDC. Calibration circuits, which contain only input and

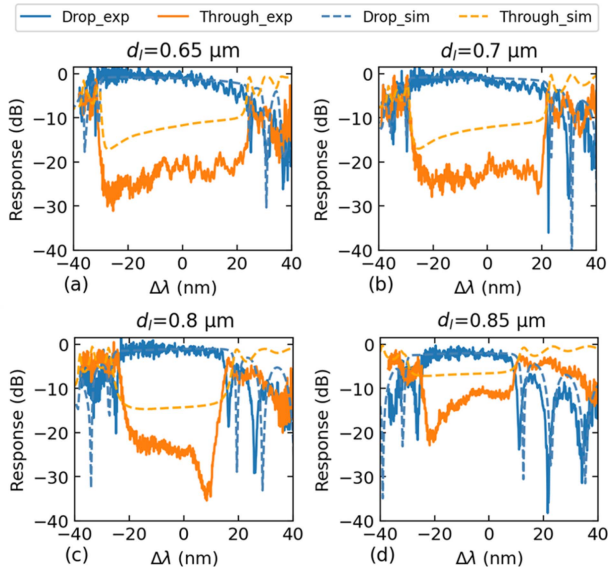


Fig. 10. Experimental responses of APhC-assisted CDCs with different d_l .

output grating couplers and an uniform waveguide connecting the two grating couplers were also fabricated and tested. The results were used to calibrate out the coupling loss of the grating couplers from the measurement results of the devices.

The APhC-assisted CDC designed in Fig. 2(a) was fabricated and characterized. This filter has been fully optimized to simultaneously provide large bandwidth, flat-top, and high ER of the spectral response. The measured result is plotted in Fig. 9(b), where the drop and through responses are plotted as blue and orange solid lines, respectively. The simulated results are also included in the figure as dashed lines for comparison. The drop response of the filter exhibits a broad and flat-top transmission band. The measured 3 dB bandwidth is 43.2 nm, which is slightly smaller than that of the simulation results (47.3 nm). The difference between the experimental and simulated bandwidths are attributed to deviations of the actual waveguide group indices and the coupling strengths from the theoretical ones caused by fabrication uncertainties. The maximum ER is ~ 25.3 dB around the center wavelength of the filter (1545 nm). This experimental ER value is smaller than that of the simulated results (51 dB), which should result from fabrication imperfections (e.g., sidewall roughness). The average insertion loss for the drop signal is calculated to be about 1.1 dB.

Then, we validate the impacts of changes in the various parameters on the CDC response obtained in the simulations. First the influence of different d_l on the CDC response is characterized. The APhC-assisted CDCs designed in Fig. 3(a)–(d), which have varying d_l , were fabricated and measured. The experimental drop and through responses of these filters are shown in Fig. 10, where the simulated responses are also included as dashed lines for comparison. It can be found that the bandwidth is decreased for a larger d_l , which is consistent with that obtained in the simulations (Fig. 3). One may notice that the experimental ERs of these filters are noticeably larger than the theoretical values. A similar phenomenon can also be found in experimental results

TABLE I
PERFORMANCE COMPARISON OF REPORTED SOI-BASED BROADBAND CDC FILTERS

Ref.	L (μm)	BW ^a (nm)	ER ^b (dB)	IL (dB)	BLR ($\times 10^{-3}$)
[14]	50	21	30	1.2	0.42
[21]	500	14	22	<2	0.03
[15]	150	33.4	35	/	0.22
[12]	374.4	32.6	>40	0.26	0.09
[16]	3200/4700	59.7/88.1	14.1/9.7	1.3/1.77	0.02/0.02
This work ^c	22.3	48.8	23.4	0.2	2.19

^a 3 dB bandwidth of the drop response.

^b Maximum extinction ratio over the operation band.

^c The filter demonstrated in Fig. 11(h) is chosen for the comparison, which has both a large bandwidth and a flat-top drop response.

L: coupling length; BW: bandwidth; ER: extinction ratio; BLR: bandwidth-to-length ratio.

of other APhC-assisted CDCs measured in this work (as we shall see in Figs. 11–14). Such larger experimental ERs compared with those obtained in the simulations could be attributed to larger practical coupling strengths over the theoretical values that may be caused by a fabrication bias of waveguide dimensions.

To verify the impact of different widths (a) and heights (b) of the elliptical nanoholes on the response of an APhC-assisted CDC, the devices designed in Fig. 5(a)–(h), which contain various a and b , were also fabricated and measured. The experimental results are shown in Fig. 11, where the simulated responses are also shown as dashed lines for comparison. The bandwidth and insertion loss as a function of a or b extracted from Fig. 11 is plotted in Fig. 12(a) or (b), respectively. As can be seen, the bandwidth is increased when a is smaller or when b is larger, and the impact of a on the spectral bandwidth is higher than that of b . These results are in good agreement with those predicted in the simulations shown in Fig. 5.

To experimentally characterize how different minimum gap between the access waveguides, g , can affect the spectral response, the APhC-assisted CDC with various g designed in Fig. 7 were fabricated and tested. The measured spectral responses of these filters are plotted in Fig. 13. The result show that the various g does not significantly affect the bandwidth of the drop response, but can change the ER and the tilt angle of the response. This is consistent with those predicted by the simulations (Fig. 7). The results confirm that g can be used to optimize the ER and the flatness of the CDC response.

The APhC-assisted CDCs with different shapes of the nanoholes designed in Fig. 8 were fabricated and measured, and the results are presented in Fig. 14. As can be seen, the circular and diamond shapes exhibit larger ERs compared with the rectangular and sinusoidal shapes, which agrees with the simulated results. The experimental drop responses of these filters show various degrees of spectral tilt, which is different from the simulation results where all filters have flat-top responses. This deviation may be attributed to the lithography smoothing effect, which could round sharp corners of nanoholes. This can influence the coupling strength of the filter, thus affecting the tilt angle of the response. The results in Fig. 14 show that the

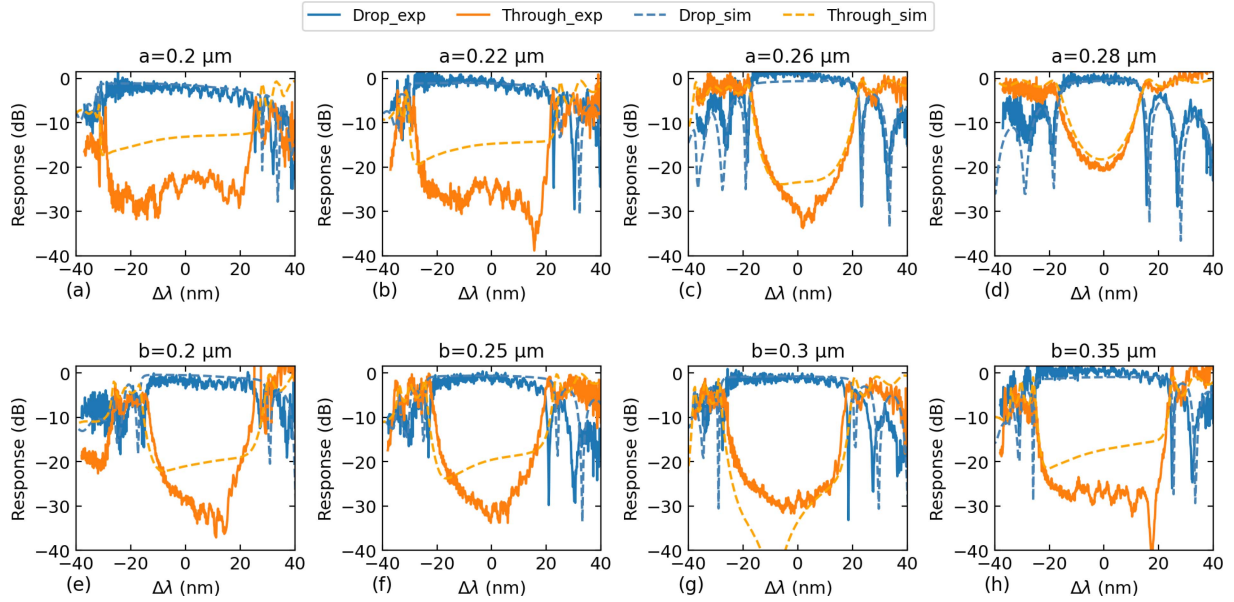


Fig. 11. Experimental responses of APhC-assisted CDCs with (a)–(d) different widths or (e)–(h) various heights of the elliptical nanoholes.

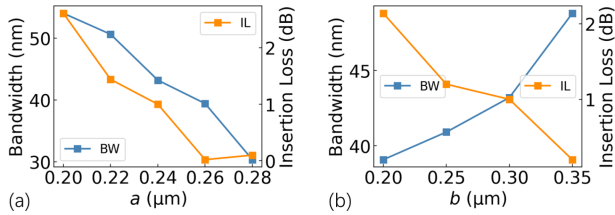


Fig. 12. Experimental 3 dB bandwidth and insertion loss of an APhC-assisted CDC as a function of (a) width (a) and (b) height (b) of the elliptical nanoholes, extracted from the experimental data shown in Fig. 11.

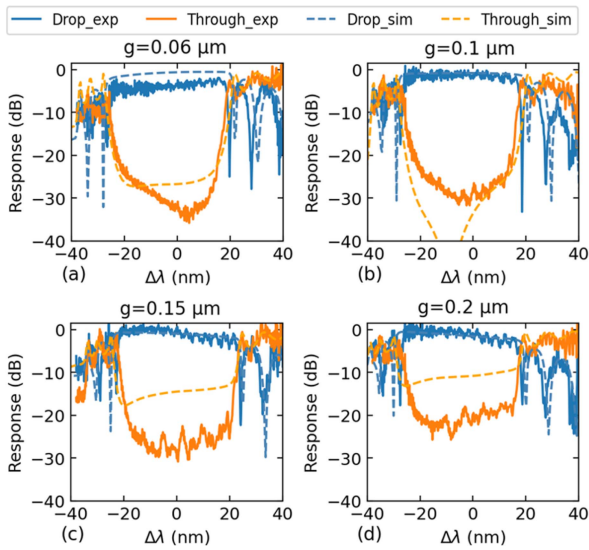


Fig. 13. Experimental responses of APhC-assisted CDCs with different minimum gaps between the access waveguides.

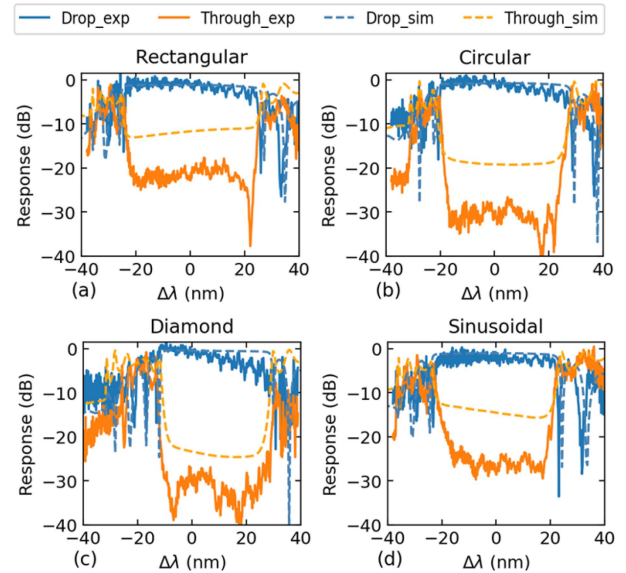


Fig. 14. Measured responses of APhC-assisted CDCs with different nanohole shapes.

degree of spectral tilt for the diamond nanohole shape is larger compared with those of the others, suggesting that this shape of the nanoholes may be most susceptible to the lithography smoothing effect.

A performance comparison between our APhC-assisted CDC and other recently reported SOI-based broadband CDC filters is given in Table I. The filter demonstrated in Fig. 11(h) is chosen for the comparison, which possesses both a large bandwidth and a flat-top drop response. The bandwidth for the drop response of the present CDC is as large as 48.8 nm. This bandwidth is only smaller than that proposed in [16], which, however,

was based on a chirped grating-assisted CDC and the device length is $>3000 \mu\text{m}$. Such a long device length could prevent its use in dense photonic integrated circuits. Besides that chirped grating-assisted CDC, our APhC-assisted CDC shows the largest bandwidth while at the same time having the most compact size and moderate ERs. The present device also possess the highest bandwidth-to-length ratio (BLR) compared with the others. The comparison highlights their great potential as broadband, flat-top, compact filters in various photonic integrated circuits.

IV. CONCLUSION

In summary, we have proposed silicon photonic CDC filters assisted by novel asymmetric multimode photonic crystals with elliptical nanoholes, which can offer significantly larger coupling strengths and thus much broader operation bandwidths compared with the conventional grating-assisted CDCs. The impacts of changes in the parameters on the CDC response have been studied, and the design and optimization method of the device have been discussed. In the experiments, a number of broadband and flat-top filters based on different APhC-assisted CDCs have been fabricated and measured. The spectral impact due to changes in the filter parameters and the design and optimization strategy have then been experimentally verified. The possibility of using other shapes of the nanoholes to implement APhC-assisted CDCs has also been explored both theoretically and experimentally. For the demonstrated filters, the achieved 3 dB bandwidth of the drop response is up to 48.8 nm, obtained with a coupling length of $22.3 \mu\text{m}$. A comparison between our device and reported broadband SOI-based CDC filters shows that the present filter possesses the largest bandwidth among all unchirped CDCs, while at the same time containing the smallest size and moderate ERs. The proposed APhC-assisted CDCs are promising candidates as broadband and flat-top 4-port filters, multiplexers, routers, etc, for various silicon photonic applications such as optical interconnects and data communications.

REFERENCES

- [1] D. Mu et al., "A four-channel DWDM tunable add/drop demultiplexer based on silicon waveguide Bragg gratings," *IEEE Photon. J.*, vol. 11, no. 1, pp. 1–8, Feb. 2019.
- [2] K. Bédard, A. D. Simard, B. Filion, Y. Painchaud, L. A. Rusch, and S. LaRochelle, "Dual phase-shift Bragg grating silicon photonic modulator operating up to 60 Gb/s," *Opt. Exp.*, vol. 24, no. 3, pp. 2413–2419, Jan. 2016.
- [3] X. Wang et al., "A silicon photonic biosensor using phase-shifted Bragg gratings in slot waveguide," *J. Biophotonics*, vol. 6, pp. 821–828, Apr. 2013.
- [4] G. Singh et al., "Resonant pumped erbium-doped waveguide lasers using distributed Bragg reflector cavities," *Opt. Lett.*, vol. 41, no. 6, pp. 1189–1192, Mar. 2016.
- [5] S. Kaushal et al., "Optical signal processing based on silicon photonics waveguide Bragg gratings: Review," *Front. Optoelectron.*, vol. 11, no. 2, pp. 163–188, Jun. 2018.
- [6] R. Cheng and L. Chrostowski, "Spectral design of silicon integrated Bragg gratings: A tutorial," *J. Lightw. Technol.*, vol. 39, no. 3, pp. 712–729, Feb. 2021.
- [7] X. Wang et al., "Hitless and gridless reconfigurable optical add drop (de)multiplexer based on looped waveguide sidewall Bragg gratings on silicon," *Opt. Exp.*, vol. 28, no. 10, pp. 14461–14475, Apr. 2020.
- [8] J. M. Castro, D. F. Geraghty, S. Honkanen, C. M. Greiner, D. Iazikov, and T. W. Mossberg, "Demonstration of mode conversion using anti-symmetric waveguide Bragg gratings," *Opt. Exp.*, vol. 13, no. 11, pp. 4180–4184, 2005.
- [9] I. Giuntioni, D. Stolarek, J. Bruns, L. Zimmermann, B. Tillack, and K. Petermann, "Integrated dispersion compensator based on apodized SOI Bragg gratings," *IEEE Photon. Technol. Lett.*, vol. 25, no. 14, pp. 1313–1316, Jul. 2013.
- [10] R. Cheng and L. Chrostowski, "Multichannel photonic hilbert transformers based on complex modulated integrated Bragg gratings," *Opt. Lett.*, vol. 43, no. 5, pp. 1031–1034, Feb. 2018.
- [11] W. Shi et al., "Silicon photonic grating-assisted, contra-directional couplers," *Opt. Exp.*, vol. 21, no. 3, pp. 3633–3650, Feb. 2013.
- [12] H. Yun, M. Hammood, S. Lin, L. Chrostowski, and N. A. F. Jaeger, "Broadband flat-top SOI adddrop filters using apodized sub-wavelength grating contradirectional couplers," *Opt. Lett.*, vol. 44, no. 20, pp. 4929–4932, Oct. 2019.
- [13] D. T. H. Tan et al., "Wide bandwidth, low loss 1 by 4 wavelength division multiplexer on silicon for optical interconnects," *Opt. Exp.*, vol. 19, no. 3, pp. 2401–2409, Jan. 2011.
- [14] B. Naghdi and L. R. Chen, "Silicon photonic contradirectional couplers using subwavelength grating waveguides," *Opt. Exp.*, vol. 24, no. 20, pp. 23429–23438, Sep. 2016.
- [15] D. Charron, J. St-Yves, O. Jafari, S. LaRochelle, and W. Shi, "Subwavelength-grating contradirectional couplers for large stopband filters," *Opt. Lett.*, vol. 43, no. 4, pp. 895–898, Feb. 2018.
- [16] M. Hammood et al., "Broadband, silicon photonic, optical adddrop filters with 3 dB bandwidths up to 11THz," *Opt. Lett.*, vol. 46, no. 11, pp. 2738–2741, May 2021.
- [17] Z. Weissman and A. Hardy, "Modes of periodically segmented waveguides," *J. Lightw. Technol.*, vol. 11, no. 11, pp. 1831–1838, Nov. 1993.
- [18] P. Yeh and H. F. Taylor, "Contradirectional frequency-selective couplers for guided-wave optics," *Appl. Opt.*, vol. 19, no. 16, pp. 2848–2855, Aug. 1980.
- [19] L. Chrostowski and M. Hochberg, *Silicon Photonics Design*. Cambridge, U.K.: Cambridge Univ. Press, Feb. 2015.
- [20] D. Wiesmann, C. David, R. Germann, D. Emi, and G. Bona, "Apodized surface-corrugated gratings with varying duty cycles," *IEEE Photon. Technol. Lett.*, vol. 12, no. 6, pp. 639–641, Jun. 2000.
- [21] J. Jiang et al., "Broadband tunable filter based on the loop of multimode Bragg grating," *Opt. Exp.*, vol. 26, no. 1, pp. 559–566, Jan. 2018.